Thermal analysis of an x-ray mask membrane in a plasma environment

M. F. Laudon, K. A. Thole, and R. L. Engelstad
Center for X-ray Lithography, University of Wisconsin–Madison, Stoughton, Wisconsin 53589

D. J. Resnick, K. D. Cummings, and W. J. Dauksher
Motorola, Inc., Tempe, Arizona 85284

(Received 19 June 1995; accepted 10 August 1995)

Quantifying the temperatures of a membrane while the mask is in a plasma environment is essential in controlling absorber stress due to deposition, and both etch rate and feature profile due to etching. Temperature gradients across the membrane during deposition lead to nonuniform stress across the absorber resulting in large distortions during pattern transfer [W. Dauksher *et al.*, J. Vac. Sci. Technol. B **13**, 3103 (1995)]. This article presents a procedure to obtain the steady state temperature profile of a mask/membrane while in a plasma environment (deposition or etch) subjected to different cooling configurations. Membrane heat fluxes and heat transfer coefficients were determined using a thermal transient technique which compares analytical solutions to experimental results. The steady state temperature profile of the membrane was then obtained by using these fluxes and heat transfer coefficients in a three-dimensional finite element model. The analysis procedure was demonstrated on a mask subjected to no helium backside cooling and a mask subjected to flowing helium backside cooling. Good agreement was obtained between the finite element solution, analytical solution, and the experimental results.

I. INTRODUCTION

The effort to achieve sub-0.25 μm x-ray lithography depends, in part, on the ability to maintain strict fabrication control leading to low distortion x-ray masks. In particular, minimizing temperature gradients within an x-ray mask membrane during plasma deposition is essential in controlling absorber properties and stress. Membrane temperature gradients and, thus, deposited metal stress gradients must be rigidly controlled in order to minimize distortions after pattern transfer. Temperature gradients over the membrane during etch can result in variations in etch rates and final etch profile. To quantify the temperature gradients in the mask, both the incident heat flux and thermal boundary conditions are needed. This article presents results from thermal transient experiments which are then used in a finite element analysis to determine the entire mask temperature profile while in a plasma environment during either deposition or etching.

There is an inherent difficulty in measuring the entire membrane temperature distribution in a plasma environment during deposition or etching. Previously reported measurements used a Luxtron fluoroptic thermometer to make a single point measurement at the membrane center for various cooling configurations.[1] Although this past study reported temperatures at the membrane center, there was no information as to the temperature gradients across the membrane. Previous analytical studies published for a mask subjected to a uniform heat flux on the surface, considered either only radial conduction or backside conduction to static helium in the gap between the mask and chuck.[2] Relatively few other related investigations have been done to determine mask temperature distributions.[3–5]

It is advantageous to predict mask temperature distributions for various cooling conditions using finite element heat transfer models. To correctly compute the temperature distribution, however, the incident heat flux, effective mask emissivity, and heat transfer coefficients are needed. In this investigation, thermal transient experiments were designed to determine the previously mentioned heat transfer characteristics. Data from the thermal transient tests were used in conjunction with analytical solutions to determine the required inputs to the finite element models. The following sections describe the experiments performed, analytical solutions, the finite element model, a comparison between measured and computed transient membrane temperatures, and steady state membrane temperature distributions.

II. EXPERIMENTAL SETUP

Typical Motorola-style x-ray masks (see Fig. 1 for mask cross section and material properties) with molybdenum thermistors (1000 Å) were fabricated, fit with lead connections and strain releases, and calibrated for various temperatures. The thermistor calibration indicated a linear relationship between resistance and temperature. These masks had 40-mm-diam silicon nitride membranes, 2.3 μm thick. The gap between the membrane and the cooling chuck was 1 mm. Figure 2 shows the thermistor layout, along with a typical thermistor mask with the leads attached. Each mask had two thermistors with one located in the center of the membrane and the second located at points labeled either 1, 2, or 3 in Fig. 2. The masks were loaded into a PlasmaTherm 770 electron cyclotron resonance (ECR) etching system and backside cooling conditions were set. Four leads per thermistor were used in order to eliminate the effect of lead resistance on the measurements. Thermistor lead wires were connected to a high speed analog-to-digital data acquisition board.

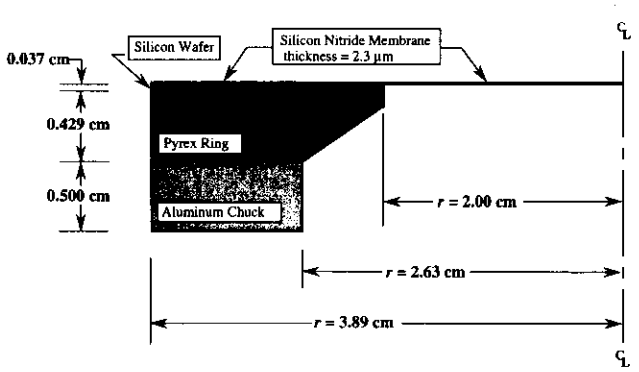

Material	Density ρ (kg/m^3)	Thermal Conductivity k (W/m/K)	Specific Heat C_v (J/kg/K)
Silicon Nitride	3440	55.6	710
Silicon	2330	155.95	701.3
Pyrex	2225	1.4	835
Aluminum	2702	237	903

FIG. 1. Schematic and material properties of the Motorola-style mask.

III. ANALYTICAL SOLUTION

Analytical solutions were derived for the thermal transient conditions imposed on the mask membrane. The objective in using these analytical solutions for the transient cases was twofold. First, the analytical solutions were used to determine the mask effective emissivity and heat transfer coefficient for a given helium flow condition. The analytical solutions were used to curve fit data for cooling the mask with radiation alone and for convection alone. Second, the analytical solutions to the thermal transient conditions were used as benchmark test cases for the finite element models.

The analytical solutions, which predict the temperature of the mask as it cools down, were based on a lumped capacitance assumption where the membrane was considered to be a constant temperature throughout. The solutions also assume that the radial conduction to the Pyrex™ ring was negligible during the cooling process and that the mask cooled more rapidly than the Pyrex ring.

For the radiation case, the mask was assumed to be small relative to the surrounding radiative area and the surrounding temperature was considered to be constant at room temperature. The resulting equation for the energy balance when the plasma is turned off is given by

$$mC_v\frac{dT_m}{dt}=-\epsilon_m A_m\sigma(T_m^4-T_b^4), \tag{1}$$

where m is the mass of the membrane, C_v is the specific heat, ϵ_m is the emissivity, A_m is the membrane area, σ is Stefan–Boltzmann's constant, and T_m and T_b are the membrane and background temperatures, respectively. Integrating this equation gives an implicit solution for time (t) as a function of temperature as given by

$$t=\frac{mC_v}{4\epsilon_m A_m\sigma T_b^3}\left\{\ln\left|\frac{T_b+T_m}{T_b-T_m}\right|-\ln\left|\frac{T_b+T_{m,i}}{T_b-T_{m,i}}\right| +2\left[\tan^{-1}\left(\frac{T_m}{T_b}\right)-\tan^{-1}\left(\frac{T_{m,i}}{T_b}\right)\right]\right\}, \tag{2}$$

where $T_{m,i}$ is the initial membrane temperature. Using the measured temperature decay, a curve fit to the data was used to determine the only unknown which is the mask emissivity, ϵ_m. After knowing the mask emissivity, the heat flux input to the mask could be obtained through an energy balance at time, $t = 0$. The heat flux to the mask was calculated from

$$q''=\sigma\epsilon_m(T_{m,i}^4-T_b^4). \tag{3}$$

For the flowing helium case, a constant heat transfer coefficient on the backside of the membrane was assumed. The resulting equation for the energy balance when the plasma is turned off is given by

$$mC_v\frac{dT_m}{dt}=-hA_m(T_m-T_f), \tag{4}$$

where h is the heat transfer coefficient and T_f is the fluid temperature. Integrating this equation gives an exponential temperature decay in the form

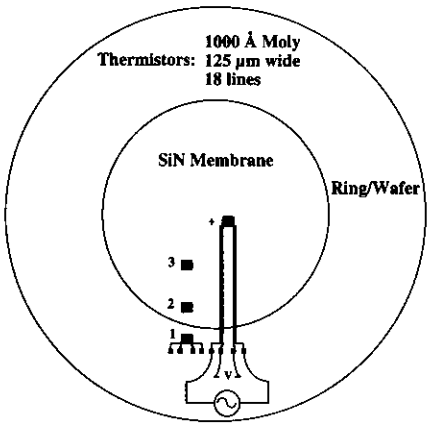

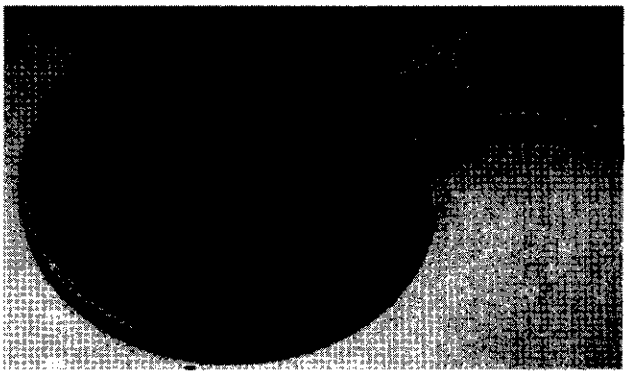

FIG. 2. Thermistor layout and an actual mask with thermistors and leads.

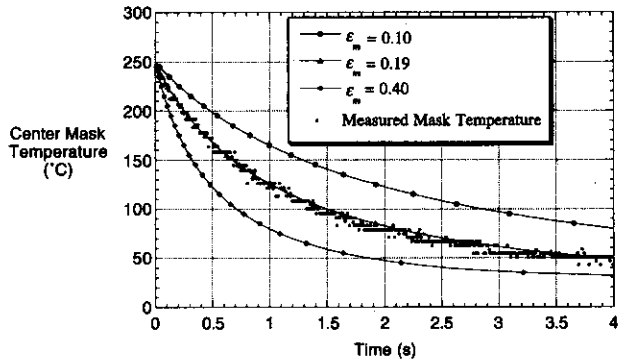

FIG. 3. Experimental and analytical membrane temperature decay after a 60 s plasma with no backside cooling on the membrane. Analytical curves for emissivity values of 0.10, 0.19, and 0.40.

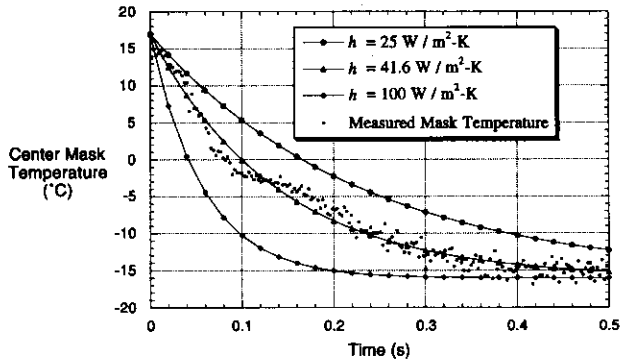

FIG. 4. Experimental and analytical membrane temperature decay after a 60 s plasma with flowing helium on the back of the membrane (P=1.19 Torr, flowrate=4.5 sccm). Analytical curves for heat transfer coefficient values of 25, 41.6, and 100 W/m^2 K.

$$T_m = T_f + (T_{m,i} - T_f)\exp\left(\frac{-hA_m}{mC_v}t\right). \quad (5)$$

Similarly, a curve fit to Eq. (5) using the measured temperature decay for the mask was used to determine the only unknown which was the heat transfer coefficient. In the actual experiments, the top side of the membrane was exposed to a vacuum. For this cooling configuration radiative cooling to the chamber was ignored and only backside cooling was taken into account. Since the heat transfer coefficient is dependent on the helium flowrate and pressure, experimental data for each condition must be analyzed to determine the correct heat transfer coefficient.

IV. MASK HEAT TRANSFER CHARACTERISTICS

Mask temperature measurements, as previously discussed, were completed to provide the surface heat flux, effective emissivity, and convective heat transfer coefficients for the finite element models. Fabricated masks were placed in the PlasmaTherm etching system and exposed to an 800 W nitrogen ECR plasma for 60 s. After the plasma was turned off, the temperature decay was measured for various cooling configurations and compared with the analytical solutions for the temperature decay. The decay data were curve fit using the appropriate analytical solution to obtain the emissivity and convective heat transfer coefficients. After knowing the mask emissivity, an energy balance was used to obtain the heat flux. As shown in Fig. 3, the effective membrane emissivity for this particular membrane was $\epsilon_m = 0.19$ and the heat flux to the mask was $q'' = 1313$ W/m^2.

Figure 4 shows that the heat transfer coefficient was $h = 41.6$ W/m^2 K for a helium flowrate of Q=4.5 sccm, pressure of $P = 1.2$ Torr, and gap width of 1 mm. Similarly, the heat flux to the mask for the flowing helium case was $q'' = 1313$ W/m^2. For this case the heat exchanger temperature had been set to -34.4 °C, however the actual temperature of the cooled flowing helium was found to be $T_f = -16$ °C. The mean free path length (λ) of helium at $P = 1.2$ Torr and a $T_f = -16$ °C is nominally λ=0.07 mm, which gives a Knudsen number of Kn=0.07. As pointed out by Mondol, Owen, and Smith,[2] when the mean free path length is greater than the gap width, Kn>1, free molecular flow occurs resulting in the heat transfer coefficient being dependent on helium pressure alone. For Kn=0.07 slip flow occurs.

V. FINITE ELEMENT MODELING

Finite element heat transfer models were developed to fully model the ring, wafer, membrane, and aluminum cooling chuck. Figure 5 shows a typical finite element model (half-model shown) used for these calculations. The support ring, aluminum chuck, and wafer were composed of eight-noded, isoparmetric, three-dimensional thermal solid elements, while the membrane was modeled with four-noded, quadrilateral thermal shell elements. Radiation was simulated using radiation link elements attached to the membrane surface, allowing for the true nonlinear solution to be obtained through iterative numerical procedures. The material properties used are listed in Fig. 1.

Boundary conditions were set depending upon the cooling condition modeled. For the cases with no backside cooling, the temperature of the aluminum chuck and the background temperature for the radiation elements were fixed at room temperature. These same boundary conditions were used for the case including flowing He backside cooling, however the appropriate heat transfer coefficient was applied to the underside of the membrane elements.

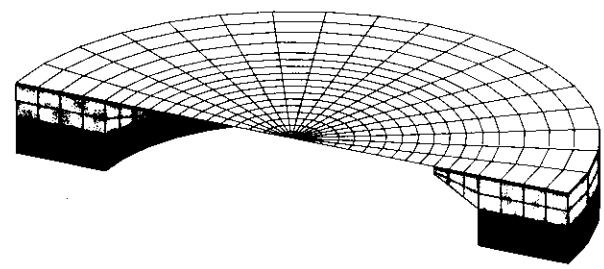

FIG. 5. Finite element thermal model of the x-ray mask (Pyrex ring, silicon wafer, silicon nitride membrane) and the aluminum cooling chuck. Models include transient and steady state radiation, convection, and radial conduction solutions.

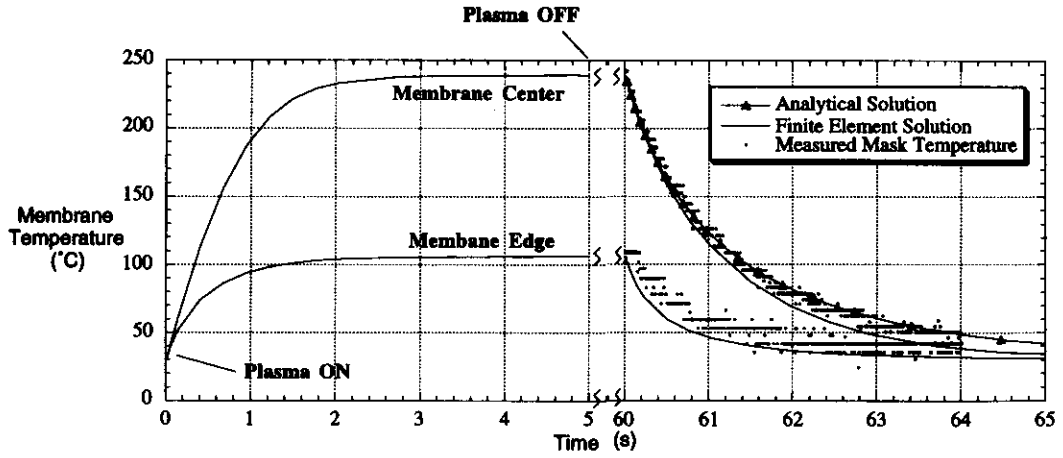

FIG. 6. Transient finite element temperature results at the center and edge of the membrane due to a plasma being struck (time=0 s) and being turned off (time=60 s). No helium backside cooling. Analytical, finite element, and experimental results are shown for the temperature decay after the plasma has been turned off.

The mask and chuck were initially set to a base temperature, and a flux was applied to the entire membrane surface (simulating the plasma) for 60 s. The flux was then shut off and the model was allowed to cool back to the base temperature. The transient temperature response of the mask/membrane was computed and compared to both the analytical solution and experimental measurements.

VI. TRANSIENT ANALYSIS USING FINITE ELEMENT MODELS

A comparison between the mask temperature decay (using the finite element model) and the measured and analytical predictions was made for both the case with no helium and flowing helium. Figure 6 shows the finite element results of the temperature decay at the membrane center and edge for the no helium case. These results were obtained using an emissivity of $\epsilon_m = 0.19$ and heat flux of $q'' = 1313$ W/m^2. The finite element model indicates a more rapid temperature decay at the edge which is a result of radial conduction. Recall, that radial conduction is not included in the analytical solution. Also, note the good agreement between the finite element model and the measured temperature decay at the edge of the membrane. The membrane edge temperature measurement is an independent check on the finite element model.

Figure 7 shows the temperature decay for the flowing helium case. These results were obtained using a heat transfer coefficient of $h = 41.6$ W/m^2 K and a heat flux of $q'' = 1313$ W/m^2. In this case, there is better agreement between the finite element model and the analytical solution, indicating that both the radial conduction at the membrane center and radiation from the top of the membrane are minimal.

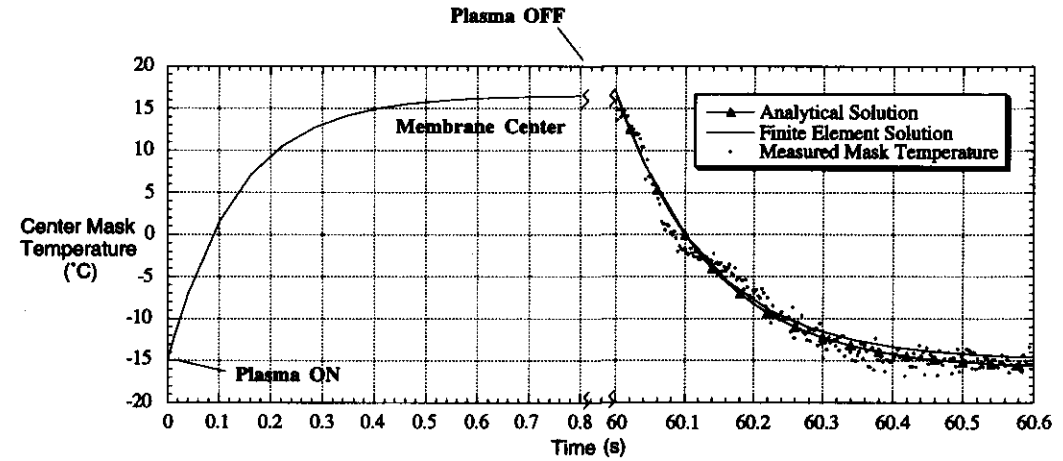

FIG. 7. Transient finite element temperature results at the center of the membrane due to a plasma being struck (time=0 s) and being turned off (time=60 s). Flowing helium backside cooling ($P = 1.19$ Torr, flowrate=4.5 sccm). Analytical, finite element, and experimental results are shown for the temperature decay after the plasma has been turned off.

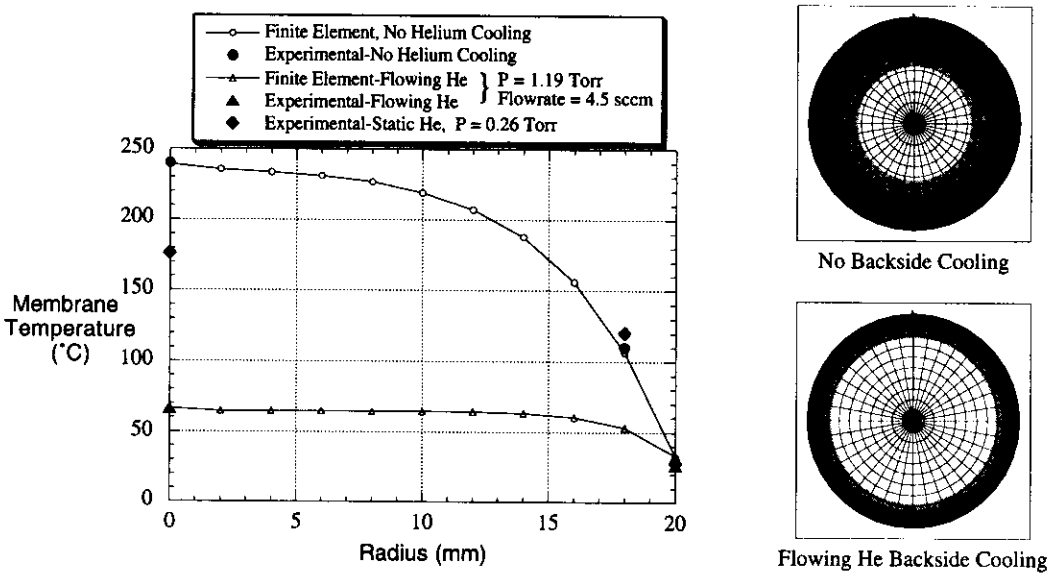

FIG. 8. Steady state membrane temperature vs radius for the no helium, flowing helium, and static helium backside cooling. Finite element results are shown both in plotted form and in contour form, for the no helium and flowing helium cases. Experimental results are shown for all three cases.

VII. STEADY STATE TEMPERATURE RESULTS

The steady state membrane temperature distribution was obtained from the finite element model using the mask heat transfer characteristics previously discussed. Figure 8 compares the radial mask temperature distribution predicted by the model with those temperatures measured just after the plasma was shut off. The computed and measured cases shown in Fig. 8 include no helium backside cooling and flowing helium backside cooling (heat exchanger set to room temperature). When no helium cooling is present, mask center temperatures reached approximately 240 °C. Experimental results only are shown for the case of static helium (P = 0.26 Torr). Temperature contours from the finite element models are shown on the right-hand side of Fig. 8. The flowing helium cooling condition produced a relatively uniform temperature profile in comparison with the no cooling case.

VIII. CONCLUSIONS

Transient temperatures were measured on a mask membrane in an etching environment after turning off the plasma to determine various heat transfer characteristics of the mask. These characteristics included the incident heat flux, effective membrane emissivity, and heat transfer coefficient for a selected helium flow condition. These temperatures were compared to analytical and finite element calculations. Good agreement was found between calculated and measured temperature decays. Using these characteristics in the finite element models, the steady-state temperature distribution in the mask was computed for both the no helium and flowing helium cases. Again, good agreement between calculated and measured temperatures was found for both cases. Based on these results, minimal temperature rise and subsequently minimal gradients occurred for the flowing helium case. Now that these experimental and computational modeling procedures have been verified, these techniques can be used to optimize the membrane cooling process and predict a usable membrane area.

ACKNOWLEDGMENTS

This research has been supported by the PXLA (Motorola, AT&T, IBM, and Loral) and the UW–Madison Center for X-ray Lithography. The Center for X-ray Lithography is supported by SRC/SEMATECH, ARPA/ONR/NRL, and the National Science Foundation.

[1]K. P. Muller, N. K. Eib, and T. B. Faure, J. Vac. Sci. Technol. B **11**, 2270 (1993).
[2]M. Mondol, G. Owen, and H. Smith, J. Vac. Sci. Technol. B **12**, 4024 (1994).
[3]M. E. Larsson and G. V. Hansson, J. Vac. Sci. Technol. A **11**, 732 (1993).
[4]M. Nakaiski, M. Yamada, and M. Nakamura, Proceedings of 1989 International Symposium on MicroProcess Conference (unpublished), pp. 93–103.
[5]M. Nakamura, T. Kurimoto, H. Yano, and K. Yanagida, 172nd Meeting of The Electrochemical Society, Honolulu, HI, October, 1987 (unpublished).